

Proximity Effects Between the Graphene Quasicrystal and Magic-Angle Twisted Bilayer Graphene

Pedro Alcazar Guerrero,^{1,2} Viet-Hung Nguyen,³ Aron W. Cummings,¹ Jean-Christophe Charlier,³ and Stephan Roche^{1,4}

¹*Catalan Institute of Nanoscience and Nanotechnology (ICN2), CSIC and BIST, Campus UAB, Bellaterra, 08193 Barcelona, Spain*

²*Department of Physics, Campus UAB, Bellaterra, 08193 Barcelona, Spain*

³*Institute of Condensed Matter and Nanosciences,*

Université catholique de Louvain (UCLouvain), 1348 Louvain-la-Neuve, Belgium

⁴*ICREA–Institució Catalana de Recerca i Estudis Avançats, 08010 Barcelona, Spain*

We report a numerical study of graphene heterostructures comprised of three individual layers twisted by either the magic angle of $\sim 1.1^\circ$, or $\sim 30^\circ$, corresponding to the graphene quasicrystal. The heterostack is modeled using realistic structural and tight-binding models, while transport properties are calculated in both clean and disordered systems containing up to ~ 8 million atoms. The weak interaction between different layers allows us to scrutinize the electronic mixing of flat bands and quasicrystalline states, which are altered differently in the low- and high-energy regimes and provide a new type of hybrid physics to be explored.

Introduction. The fascinating discovery of the superconducting and Mott insulating phases in magic-angle twisted bilayer graphene (MATBLG) has generated a huge interest in deepening our understanding of the physics of flat-band systems, where a dominant Coulomb interaction triggers a wealth of emerging many-body phenomena [1–17]. In parallel, a “graphene quasicrystal” for a twist angle of 30° between two graphene layers has been observed [18], and later grown deterministically via chemical vapor deposition [19], eliminating the need for artificial assembly. In the decades after their first experimental observation [20], the realization of quasicrystalline structures has captivated material scientists for their quasiperiodic tiling with self-similar properties [21–24]. Very recently, other generalizations of Moiré quasicrystals have been also discovered [25, 26].

While the exotic physics of MATBLG is dominated by low-energy flat bands, the peculiar electronic states in graphene quasicrystals are to date mainly found at high energies, and the low-energy region seems to be well described by the physics of the individual graphene layers. The combination of both types of stacking could thus generate a strange mixture of “two different worlds,” which are separately still under intense investigation.

The graphene quasicrystal is by definition aperiodic, which complicates the study of its electronic properties. The juxtaposition of MATBLG with a graphene quasicrystal presents further computational issues, owing to the absence of translational invariance combined with the large unit cell of MATBLG. One can construct quasicrystalline approximant structures that are periodic but which share electronic similarities with the aperiodic quasicrystal [27, 28], but the system size quickly increases to millions of atoms as the chosen angle approaches 30° . This makes a theoretical exploration of those structures, as well as their disordered variants, out of the reach of conventional computational approaches, hence limit-

ing the inspection of possible undiscovered properties of “MATBLG/graphene quasicrystal” hybrid stacks.

In this Letter, we overcome these difficulties by implementing a realistic tight-binding model which describes the electronic properties of graphene layers stacked at both the magic angle and the quasicrystalline approximant twist angles. In combination with an efficient linear-scaling approach [29], we simulate the electronic transport properties of MATBLG/graphene quasicrystal trilayer stacks containing up to ~ 8 million atoms, thus allowing for the first time the study of the respective modifications of flat bands and quasicrystalline-like states driven by proximity effects.

In the absence of disorder, the flat bands of MATBLG are found to be unaffected by the quasicrystalline states. This contrasts with the high-energy quasicrystalline states, which are suppressed by the interaction with MATBLG. However, when introducing disorder we see the opposite effect. In this case, in the low-energy flat bands we observe a reversal of the recently discovered disorder-induced delocalization in MATBLG [30]. Meanwhile, in the high-energy quasicrystalline states, the transport properties are unaffected by the presence of the magic-angle graphene layer.

Structural optimization and tight-binding model. The atomic structures of graphene superlattices at the magic angle and at the quasicrystal approximant angles were relaxed using molecular dynamics simulations with classical potentials [31, 32]. Intralayer forces were computed using the optimized Tersoff potentials [33], whereas interlayer forces were modeled using the Kolmogorov–Crespi potentials [34, 35]. The atomic structures were optimized until all force components were smaller than $0.5 \text{ meV}/\text{\AA}$. To model quasicrystalline graphene, we consider two approximant angles close to 30° , namely 31° and 29.8° [27]. These approximants share similarities with the fully aperiodic quasicrystal, such as the formation of high energy

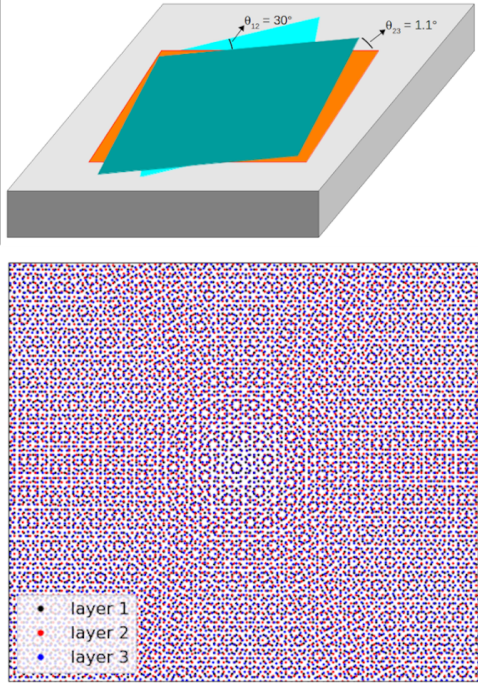


FIG. 1. Schematic of twisted multilayer graphene systems on a flat substrate such as bulk h-BN (top panel), and top view of the atomic structure of the trilayer stack (bottom panel). Patterns reminiscent of the AA (center region) and AB zones of MATBLG and the 12-fold rotational structures of the quasicrystalline approximant are visible.

states whose real space projections exhibit dodecagonal symmetry [18].

Twisted graphene systems are often deposited on a substrate which could have a flat surface, such as h-BN [36] (see Fig. 1). The interaction between the flat substrate and the bottom graphene layer can diminish the moiré-induced corrugation in this layer. For this reason, both free-standing graphene and graphene on a substrate are investigated. In the former case, all C-atoms can freely move during the relaxation calculation. In the latter case, C-atoms can move under the condition that the bottom graphene layer is kept flat. In our simulations of electronic properties, we have found a negligible difference between these structures.

The electronic properties of twisted graphene systems are then computed using the p_z tight-binding (TB) Hamiltonian elaborated in [31, 32]. The hopping energies t_{nm} between carbon n - and m -sites are determined by the standard Slater-Koster formula

$$t_{nm} = \cos^2 \phi_{nm} V_{pp\sigma}(r_{nm}) + \sin^2 \phi_{nm} V_{pp\pi}(r_{nm}),$$

where the direction cosine of $\vec{r}_{nm} = \vec{r}_m - \vec{r}_n$ along the z axis is $\cos \phi_{nm} = z_{nm}/r_{nm}$. The distance-dependent

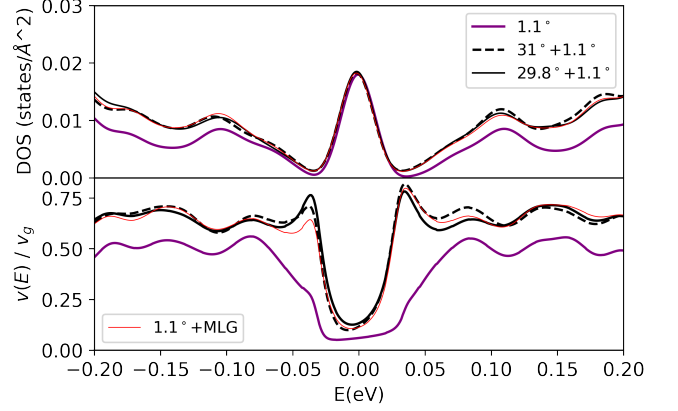


FIG. 2. Density of states (top panel) and Fermi velocities (bottom panel) of MATBLG (purple solid line) and the two trilayer systems (black solid and dashed lines). The averaged Fermi velocity of the trilayer system is depicted by the red line, considering a trilayer system where the MATBLG and the quasicrystalline layer are decoupled (see main text).

Slater-Koster parameters are determined as [37, 38]

$$V_{pp\pi}(r_{nm}) = V_{pp\pi}^0 \exp \left[q_{\pi} \left(1 - \frac{r_{nm}}{a_0} \right) \right] F_c(r_{nm}),$$

$$V_{pp\sigma}(r_{nm}) = V_{pp\sigma}^0 \exp \left[q_{\sigma} \left(1 - \frac{r_{nm}}{d_0} \right) \right] F_c(r_{nm}),$$

with a smooth cutoff function $F_c(r_{nm}) = [1 + \exp((r_{nm} - r_c)/\lambda_c)]^{-1}$. Note that here we use a cutoff of electronic couplings, $r_{\text{inplane}} \leq 0.432$ nm [32]. This approximation results in a highly sparse TB Hamiltonian matrix, making calculations feasible for small twist angles and/or multilayered systems with a large number of atoms. Within this approximation, the adjusted TB parameters are $V_{pp\pi}^0 = -2.7$ eV, $V_{pp\sigma}^0 = 367.5$ meV, $\frac{q_{\pi}}{a_0} = \frac{q_{\sigma}}{d_0} = 22.18$ nm⁻¹, $a_0 = 0.1439$ nm, $d_0 = 0.33$ nm, $r_c = 0.614$ nm, and $\lambda_c = 0.0265$ nm. To model disorder, a random Anderson potential uniformly distributed within $[-W/2, +W/2]$ is added to the onsite energies of the p_z orbitals.

Calculation of electronic properties. We use an efficient linear-scaling quantum transport methodology [29] to study the electronic properties of the MATBLG/quasicrystal trilayer stacks. For transport, the main quantity we calculate is the mean square displacement of an initial state $|\psi(0)\rangle$, given by

$$\Delta X^2(E, t) = \frac{\langle \psi_X(t) | \delta(E - \hat{H}) | \psi_X(t) \rangle}{\rho(E)},$$

where \hat{H} is the TB Hamiltonian, $|\psi_X(t)\rangle = [\hat{X}, \hat{U}(t)] |\psi(0)\rangle$, \hat{X} is the position operator, $\hat{U}(t) = \exp(-i\hat{H}t/\hbar)$ is the time evolution operator, and $\rho(E) = \langle \psi(0) | \delta(E - \hat{H}) | \psi(0) \rangle$ is the density of states (DOS). To

avoid direct diagonalization, the time evolution operator and the energy projection operator $\delta(E - \hat{H})$ are expanded as a series of Chebyshev polynomials. The initial state $|\psi(0)\rangle$ is a random-phase state that permits efficient calculation of electronic properties over the full Hamiltonian spectrum [39]. From the mean square displacement we extract the diffusion coefficient $D(E, t) = \frac{1}{2} \frac{\partial}{\partial t} \Delta X^2(E, t)$. In the ballistic regime we extract the Fermi velocity via $D(E, t) = v^2(E)t$, while with disorder the mean free path can be deduced from $\ell(E) = 2D_{\max}(E)/v(E)$, where $D_{\max}(E) = \max_t D(E, t)$.

We use timesteps of 10 and 1 fs for transport in the clean and disorder systems, respectively. We expand $\delta(E - \hat{H})$ as a series of 3500 Chebyshev polynomials with the Jackson kernel [39], corresponding to a Gaussian energy broadening of ~ 23 meV. The trilayer systems contain a total of ~ 5 million atoms for the 31° approximant and ~ 8 million atoms for the 29.8° approximant.

Low-energy regime and flat-band states. We first examine the low-energy flat-band states in MATBLG, and how they are modified by adding a $\sim 30^\circ$ -rotated graphene layer. In Fig. 2 (top panel), we plot the DOS of MATBLG and each of the two MATBLG/quasicrystal approximants, focusing on the low-energy regime. In the flat-band region, $|E| \lesssim 25$ meV, the DOS is nearly identical for all three cases, while a small increase is seen at larger energies for the trilayer structures.

In the bottom panel of Fig. 2, we plot the Fermi velocity of each system. Here we see a substantial modification of ballistic transport between the bi- and trilayer cases, manifesting as a significant increase of the Fermi velocity (up to $5\times$) in the trilayer case. However, our methodology calculates the Fermi velocity averaged over the entire Fermi surface, and this result may thus arise from the average of parallel transport in the MATBLG layers at velocity v_{MA} and a decoupled quasicrystalline layer at v_g . To check this, we have made calculations for a decoupled system by removing all interlayer interactions between the MATBLG and the bottom graphene layer. This corresponds to the red curve in Fig. 2, where we see no significant difference arise at low energy for the DOS nor for the Fermi velocity.

This observation is consistent with the layer-projected DOS and local DOS (LDOS) in each of the layers, shown in Fig. 3. Here we see that the DOS of the MATBLG layers (middle and top layers) exhibits the flat-band peak at $E = 0$, while the quasicrystal layer (bottom layer) resembles single-layer graphene. Similarly, the LDOS of the MATBLG layers exhibits the characteristic moiré periodicity, with states localized in the AA overlap regions, while the quasicrystal layer shows no evidence of the moiré superlattice.

The above results have shown that, in the clean limit, adding a $\sim 30^\circ$ -rotated graphene layer to MATBLG has little impact on the low-energy flat-band states. We now

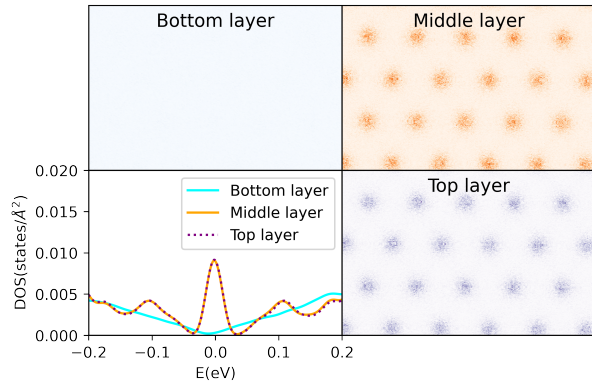


FIG. 3. Layer-projected DOS (bottom left panel) and LDOS of each of the layers for the $31^\circ+1.1^\circ$ trilayer hybrid system at charge neutrality ($E = 0$). The moiré pattern is visible in the two 1.1° -rotated layers, while the extra quasicrystalline layer does not display any signal of the flat band.

see if this extends to transport in the presence of disorder. We consider Anderson disorder values, $W = 3V_{pp\pi}^0/4$ and $6V_{pp\pi}^0/4$, where we see an anomalous disorder-induced delocalization in MATBLG, as discovered in Ref. 30. We reproduce these results in the inset of Fig. 4, where we show the time evolution of the diffusion coefficient of MATBLG in the middle of the flat band ($E = 0$). Here we see that when increasing the disorder strength, we see an anomalous increase in D at long times.

This situation is strongly altered in the trilayer case, as shown in the main panel of Fig. 4. Here we see that at long times, increasing the disorder strength always reduces the diffusion coefficient. The anomalous disorder-induced delocalization seen in MATBLG thus appears to be suppressed when adding a quasicrystalline graphene layer to the stack, resulting in “standard” transport behavior. This occurs despite the strong resilience of the state projection on the MATBLG layers in the clean case.

High-energy regime and quasicrystalline states. We now focus on the electronic structure and transport in the high-energy regime. Here we obtain a favorable comparison to prior results on graphene quasicrystalline approximants [27, 40], which have demonstrated the presence of resonant peaks in the DOS at energies between -2 and -1.5 eV, including the so-called α -peak shown as the vertical dotted line in Fig. 5. These peaks correspond to localized states lacking spatial periodicity and displaying quasiperiodic orientational patterns. The top panel of Fig. 5 shows that adding an extra 1.1° -rotated layer on top of the quasicrystalline stack leads to strong suppression of the quasicrystalline fingerprints in the DOS.

Figure 5 (bottom panel) shows the corresponding normalized Fermi velocity of each structure. Consistent with the suppression of the resonant peaks in the DOS, the velocity profile also becomes relatively featureless with the

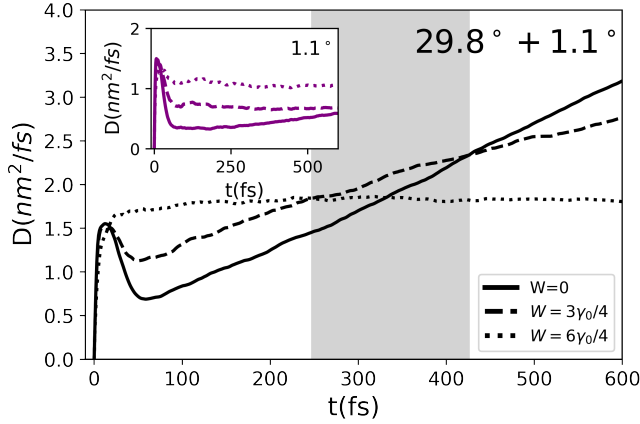


FIG. 4. Time-dependent diffusion coefficient in the flat band for different disorder strengths, for MATBLG (inset) and the trilayer with the 29.8° approximant (main panel).

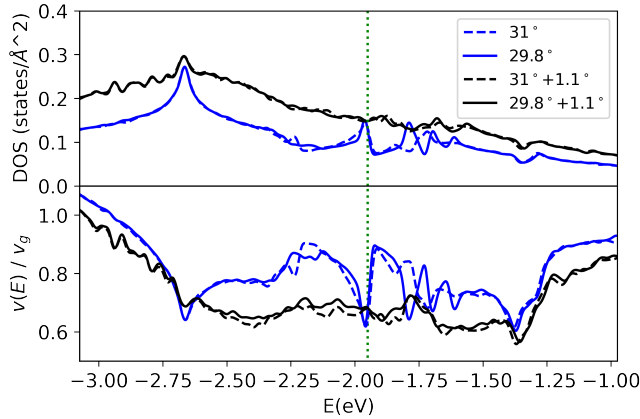


FIG. 5. DOS (top panel) and Fermi velocity (bottom panel) in the high-energy quasicrystalline-state regime. The vertical green dotted line marks the energy of the α quasicrystalline peak ($E = -1.95$ eV) [27].

addition of the 1.1° -rotated layer. Overall, the additional layer induces a reduction of the Fermi velocity throughout the entire energy range of interest.

Finally, we focus on transport in the high-energy regime, where the formation of resonant quasicrystalline states has been observed experimentally and is well reproduced theoretically. At those resonance energies, the real-space extension of the electronic states indicates the emergence of dodecagonal ordering (incompatible with translational invariance), which could point towards unconventional electronic features in the limit of a totally aperiodic structure, as known for other quasicrystalline structures [41–46]. Our simulations, however, do not reveal any unusual transport behavior in the graphene quasicrystalline approximant. As shown in Fig. 6, Anderson disorder leads to standard diffusive behavior, with stronger disorder leading to slower diffusion and a re-

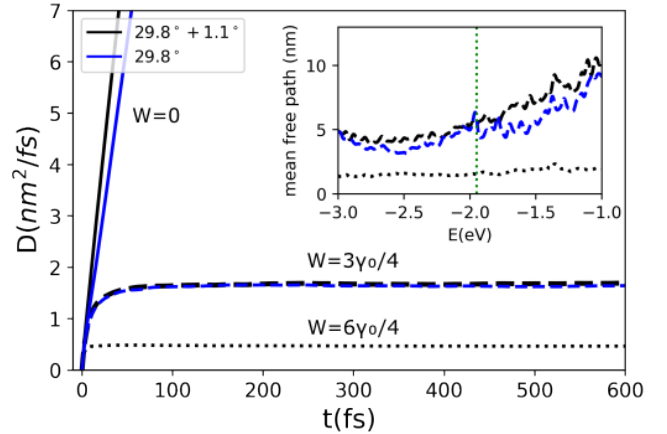


FIG. 6. Time-dependent diffusion coefficient of the quasicrystalline approximant and the trilayer system at the energy of the α -peak (vertical dotted line in the inset and in Fig. 5). Inset: energy-dependent mean free path of both systems. The vertical dotted line marks the position of the quasicrystal α -peak.

duced mean free path (shown in the inset). We also find that, in contrast to the DOS and the Fermi velocity in the clean case, adding a 1.1° -rotated layer has minimal impact on transport in the presence of disorder.

Summary and conclusions. We have shown that interfacing MATBLG with graphene quasicrystal approximants leads to a variety of proximity effects. While the low-energy flat-band states appear to be insensitive to the addition of a $\sim 30^\circ$ -rotated layer in the clean case, the high-energy quasicrystalline states are suppressed by the presence of a magic-angle layer. Meanwhile, adding disorder reveals the opposite trend. In the low-energy regime, the proximity effect suppresses the anomalous disorder-induced delocalization discovered in the flat bands of MATBLG [30]. However, in the high-energy regime, disorder does not lead to any transport anomalies in the quasicrystal states, independent of the presence of the magic-angle layer. This contrasts with the physics of intermetallic alloys-based quasicrystals, where disorder-induced delocalization remains a long-standing conundrum [41, 47, 48]. Looking ahead, it would be instructive to deepen the study of disorder effects in light of recent developments in other quasicrystalline systems [42–46].

ICN2 is funded by the CERCA Programme/Generalitat de Catalunya and supported by the Severo Ochoa Centres of Excellence programme, Grant CEX2021-001214-S, funded by MCIN/AEI/10.13039.501100011033. This work is also supported by MICIN with European funds-NextGenerationEU (PRTR-C17.11) and by 2021 SGR 00997, funded by Generalitat de Catalunya. V.-H.N. and J.-C.C. acknowledge financial support from the

Fédération Wallonie-Bruxelles through the ARC Grant “DREAMS” (No. 21/26-116), from the EOS project “CONNECT” (No. 40007563), from the EU Pathfinder project “FLATS” (No. 101099139), and from the Belgium F.R.S.-FNRS through the research project (No. T.029.22F). Simulations were performed at the Center for Nanoscale Materials, a U.S. Department of Energy Office of Science User Facility, supported by the U.S. DOE, Office of Basic Energy Sciences, under Contract No. 83336. Computational resources were also provided by the supercomputing facilities of UCLouvain (CISM) and the Consortium des Équipements de Calcul Intensif (CÉCI), funded by the F.R.S.-FNRS under Grant No. 2.5020.11 and by the Walloon Region.

-
- [1] Y. Cao, V. Fatemi, S. Fang, K. Watanabe, T. Taniguchi, E. Kaxiras, and P. Jarillo-Herrero, Unconventional superconductivity in magic-angle graphene superlattices, *Nature* **556**, 43 (2018).
- [2] Y. Cao, V. Fatemi, A. Demir, S. Fang, S. L. Tomarken, J. Y. Luo, J. D. Sanchez-Yamagishi, K. Watanabe, T. Taniguchi, E. Kaxiras, R. C. Ashoori, and P. Jarillo-Herrero, Correlated insulator behaviour at half-filling in magic-angle graphene superlattices, *Nature* **556**, 80 (2018).
- [3] P. Stepanov, I. Das, X. Lu, A. Fahimniya, K. Watanabe, T. Taniguchi, F. H. L. Koppens, J. Lischner, L. Levitov, and D. K. Efetov, Untying the insulating and superconducting orders in magic-angle graphene, *Nature* **583**, 375 (2020).
- [4] R. Bistritzer and A. H. MacDonald, Moiré bands in twisted double-layer graphene, *Proc. Natl. Acad. Sci. U.S.A.* **108**, 12233 (2011).
- [5] E. Y. Andrei, D. K. Efetov, P. Jarillo-Herrero, A. H. MacDonald, K. F. Mak, T. Senthil, E. Tutuc, A. Yazdani, and A. F. Young, The marvels of moiré materials, *Nat. Rev. Mater.* **6**, 201 (2021).
- [6] N. Tilak, X. Lai, S. Wu, Z. Zhang, M. Xu, R. d. A. Ribeiro, P. C. Canfield, and E. Y. Andrei, Flat band carrier confinement in magic-angle twisted bilayer graphene, *Nat. Commun.* **12**, 4180 (2021).
- [7] M. Serlin, C. L. Tschirhart, H. Polshyn, Y. Zhang, J. Zhu, K. Watanabe, T. Taniguchi, L. Balents, and A. F. Young, Intrinsic quantized anomalous hall effect in a moiré heterostructure, *Science* **367**, 900 (2020).
- [8] Y. Saito, J. Ge, K. Watanabe, T. Taniguchi, and A. F. Young, Independent superconductors and correlated insulators in twisted bilayer graphene, *Nat. Phys.* **16**, 926 (2020).
- [9] L. Balents, C. R. Dean, D. K. Efetov, and A. F. Young, Superconductivity and strong correlations in moiré flat bands, *Nat. Phys.* **16**, 725 (2020).
- [10] P. Stepanov, M. Xie, T. Taniguchi, K. Watanabe, X. Lu, A. H. MacDonald, B. A. Bernevig, and D. K. Efetov, Competing zero-field chern insulators in superconducting twisted bilayer graphene, *Phys. Rev. Lett.* **127**, 197701 (2021).
- [11] Y. Xie, A. T. Pierce, J. M. Park, D. E. Parker, E. Khalaf, P. Ledwith, Y. Cao, S. H. Lee, S. Chen, P. R. Forrester, K. Watanabe, T. Taniguchi, A. Vishwanath, P. Jarillo-Herrero, and A. Yacoby, Fractional chern insulators in magic-angle twisted bilayer graphene, *Nature* **600**, 439 (2021).
- [12] A. T. Pierce, Y. Xie, J. M. Park, E. Khalaf, S. H. Lee, Y. Cao, D. E. Parker, P. R. Forrester, S. Chen, K. Watanabe, T. Taniguchi, A. Vishwanath, P. Jarillo-Herrero, and A. Yacoby, Unconventional sequence of correlated chern insulators in magic-angle twisted bilayer graphene, *Nat. Phys.* **17**, 1210 (2021).
- [13] Y. H. Kwan, Y. Hu, S. H. Simon, and S. A. Parameswaran, Exciton band topology in spontaneous quantum anomalous hall insulators: Applications to twisted bilayer graphene, *Phys. Rev. Lett.* **126**, 137601 (2021).
- [14] J. M. Park, Y. Cao, L.-Q. Xia, S. Sun, K. Watanabe, T. Taniguchi, and P. Jarillo-Herrero, Robust superconductivity in magic-angle multilayer graphene family, *Nat. Mater.* **21**, 877 (2022).
- [15] A. Jaoui, I. Das, G. Di Battista, J. Díez-Mérida, X. Lu, K. Watanabe, T. Taniguchi, H. Ishizuka, L. Levitov, and D. K. Efetov, Quantum critical behaviour in magic-angle twisted bilayer graphene, *Nat. Phys.* **18**, 633 (2022).
- [16] A. K. Paul, A. Ghosh, S. Chakraborty, U. Roy, R. Dutta, K. Watanabe, T. Taniguchi, A. Panda, A. Agarwala, S. Mukerjee, S. Banerjee, and A. Das, Interaction-driven giant thermopower in magic-angle twisted bilayer graphene, *Nat. Phys.* **18**, 691 (2022).
- [17] D. R. Klein, L.-Q. Xia, D. MacNeill, K. Watanabe, T. Taniguchi, and P. Jarillo-Herrero, Electrical switching of a bistable moiré superconductor, *Nat. Nanotechnol.* **18**, 331 (2023).
- [18] S. J. Ahn, P. Moon, T.-H. Kim, H.-W. Kim, H.-C. Shin, E. H. Kim, H. W. Cha, S.-J. Kahng, P. Kim, M. Koshino, Y.-W. Son, C.-W. Yang, and J. R. Ahn, Dirac electrons in a dodecagonal graphene quasicrystal, *Science* **361**, 782 (2018).
- [19] S. Pezzini, V. Mišeikis, G. Piccinini, S. Forti, S. Pace, R. Engelke, F. Rossella, K. Watanabe, T. Taniguchi, P. Kim, and C. Coletti, 30°-twisted bilayer graphene quasicrystals from chemical vapor deposition, *Nano Lett.* **20**, 3313 (2020).
- [20] D. Shechtman, I. Blech, D. Gratias, and J. W. Cahn, Metallic phase with long-range orientational order and no translational symmetry, *Phys. Rev. Lett.* **53**, 1951 (1984).
- [21] D. Levine and P. J. Steinhardt, Quasicrystals: A new class of ordered structures, *Phys. Rev. Lett.* **53**, 2477 (1984).
- [22] E. Maciá, The role of aperiodic order in science and technology, *Rep. Prog. Phys.* **69**, 397 (2005).
- [23] L. Bindi, P. J. Steinhardt, N. Yao, and P. J. Lu, Natural quasicrystals, *Science* **324**, 1306 (2009).
- [24] L. Bindi and G. Parisi, Quasicrystals: fragments of history and future outlooks, *Rend. Lincei. Sci. Fis.* **34**, 317 (2023).
- [25] A. Uri, S. C. de la Barrera, M. T. Randeria, D. Rodan-Legrain, T. Devakul, P. J. D. Crowley, N. Paul, K. Watanabe, T. Taniguchi, R. Lifshitz, L. Fu, R. C. Ashoori, and P. Jarillo-Herrero, Superconductivity and strong interactions in a tunable moiré quasicrystal, *Nature* **620**, 762 (2023).
- [26] X. Lai, D. Guerci, G. Li, K. Watanabe, T. Taniguchi, J. Wilson, J. H. Pixley, and E. Y. Andrei, Imag-

- ing self-aligned moiré crystals and quasicrystals in magic-angle bilayer graphene on hbn heterostructures, [arXiv:2311.07819](#).
- [27] P. Moon, M. Koshino, and Y.-W. Son, Quasicrystalline electronic states in 30° rotated twisted bilayer graphene, *Phys. Rev. B* **99**, 165430 (2019).
- [28] G. Yu, Z. Wu, Z. Zhan, M. I. Katsnelson, and S. Yuan, Dodecagonal bilayer graphene quasicrystal and its approximants, *Npj Comput. Mater.* **5**, 122 (2019).
- [29] Z. Fan, J. H. Garcia, A. W. Cummings, J. E. Barrios-Vargas, M. Panhans, A. Harju, F. Ortmann, and S. Roche, Linear scaling quantum transport methodologies, *Phys. Rep.* **903**, 1 (2021), linear scaling quantum transport methodologies.
- [30] P. A. Guerrero, V.-H. Nguyen, J. M. Romeral, A. W. Cummings, J.-H. Garcia, J.-C. Charlier, and S. Roche, Disorder-induced delocalization in magic-angle twisted bilayer graphene, [arXiv:2401.08265](#).
- [31] V. H. Nguyen, D. Paszko, M. Lamparski, B. V. Troeye, V. Meunier, and J.-C. Charlier, Electronic localization in small-angle twisted bilayer graphene, *2D Mater.* **8**, 035046 (2021).
- [32] V. H. Nguyen, T. X. Hoang, and J.-C. Charlier, Electronic properties of twisted multilayer graphene, *J. Phys. Mater.* **5**, 034003 (2022).
- [33] L. Lindsay and D. A. Broido, Optimized tersoff and brenner empirical potential parameters for lattice dynamics and phonon thermal transport in carbon nanotubes and graphene, *Phys. Rev. B* **81**, 205441 (2010).
- [34] A. N. Kolmogorov and V. H. Crespi, Registry-dependent interlayer potential for graphitic systems, *Phys. Rev. B* **71**, 235415 (2005).
- [35] I. Leven, T. Maaravi, I. Azuri, L. Kronik, and O. Hod, Interlayer potential for graphene/h-bn heterostructures, *J. Chem. Theory Comput.* **12**, 2896 (2016).
- [36] C. R. Dean, A. F. Young, I. Meric, C. Lee, L. Wang, S. Sorgenfrei, K. Watanabe, T. Taniguchi, P. Kim, K. L. Shepard, and J. Hone, Boron nitride substrates for high-quality graphene electronics, *Nat. Nanotechnol.* (2010).
- [37] G. Trambly de Laissardière, D. Mayou, and L. Magaud, Localization of dirac electrons in rotated graphene bilayers, *Nano Lett.* **10**, 804 (2010), pMID: 20121163.
- [38] G. Trambly de Laissardière, D. Mayou, and L. Magaud, Numerical studies of confined states in rotated bilayers of graphene, *Phys. Rev. B* **86**, 125413 (2012).
- [39] A. Weiße, G. Wellein, A. Alvermann, and H. Fehske, The kernel polynomial method, *Rev. Mod. Phys.* **78**, 275 (2006).
- [40] J. A. Crosse and P. Moon, Quasicrystalline electronic states in twisted bilayers and the effects of interlayer and sublattice symmetries, *Phys. Rev. B* **103**, 045408 (2021).
- [41] S. Roche, G. Trambly de Laissardière, and D. Mayou, Electronic transport properties of quasicrystals, *J. Math. Phys.* **38**, 1794 (1997).
- [42] A. Moustaj, S. Kempkes, and C. M. Smith, Effects of disorder in the fibonacci quasicrystal, *Phys. Rev. B* **104**, 144201 (2021).
- [43] C.-B. Hua, Z.-R. Liu, T. Peng, R. Chen, D.-H. Xu, and B. Zhou, Disorder-induced chiral and helical majorana edge modes in a two-dimensional ammann-beenker quasicrystal, *Phys. Rev. B* **104**, 155304 (2021).
- [44] T. Peng, Y.-C. Xiong, C.-B. Hua, Z.-R. Liu, X. Zhu, W. Cao, F. Lv, Y. Hou, B. Zhou, Z. Wang, and R. Xiong, Structural disorder-induced topological phase transitions in quasicrystals, [arXiv:2403.04338](#).
- [45] A. Jagannathan and M. Tarzia, Electronic states of a disordered two-dimensional quasiperiodic tiling: From critical states to anderson localization, *Phys. Rev. B* **107**, 054206 (2023).
- [46] J. Schirmann, S. Franca, F. Flicker, and A. G. Grushin, Physical properties of an aperiodic monotile with graphene-like features, chirality, and zero modes, *Phys. Rev. Lett.* **132**, 086402 (2024).
- [47] S. Roche and D. Mayou, Conductivity of quasiperiodic systems: A numerical study, *Phys. Rev. Lett.* **79**, 2518 (1997).
- [48] S. Roche and T. Fujiwara, Fermi surfaces and anomalous transport in quasicrystals, *Phys. Rev. B* **58**, 11338 (1998).